LA-UR-84-3577

CONF-850136--2

Los Alamos National Laboratory is operated by the University of California for the United States Department of Energy under contract W-7405-ENG-36.

LA-UR--84-3577

DE85 003733

TITLE: Los Alamos Energetic Particle Sensor Systems at Geostationary Orbit

AUTHOR(S): D.N. Baker, W. Aiello, J.R. Asbridge, R.D. Belian, P.R. Higbie, R.W. Klebesadel, J.G. Laros and E.R. Tech

SUBMITTED TO: AIAA 23rd Aerospace Sciences Meeting in Reno, Nevada, 14-17 January 1985

DISCLAIMER

Los Alamos National Laboratory
Los Alamos, New Mexico 87545

FORM NO. 836 R4

LOS ALAMOS ENERGETIC PARTICLE SENSOR SYSTEMS AT GEOSTATIONARY ORBIT

D. N. Baker, W. Aiello, J. R. Asbridge, R. D. Belian, P. R. Higbie,
R. W. Klebesadel, J. G. Laros, and E. R. Tech
University of California, Los Alamos National Laboratory
Los Alamos, New Mexico 87545

Abstract

The Los Alamos National Laboratory has provided energetic particle sensors for a variety of spacecraft at the geostationary orbit (36,000 km altitude). The sensor system called the Charged Particle Analyzer (CPA) consists of four separate subsystems. The LoE and HiE subsystems measure electrons in the energy ranges 30-300 keV and 200-2000 keV, respectively. The LoP and HiP subsystems measure ions in the ranges 100-600 keV and 0.4-150 MeV, respectively. A separate sensor system called the spectrometer for energetic electrons (SEE) measures very high-energy electrons (2-15 MeV) using advanced scintillator design. In this paper we describe the relationship of operational anomalies and spacecraft upsets to the directly measured energetic particle environments at 6.6 R_E. We also compare and contrast the CPA and SEE instrument design characteristics with the next generation of Los Alamos instruments to be flown at geostationary altitudes.

Introduction

Spacecraft operating, within the earth's magnetosphere generally are subjected to a hostile environment due to charged particle radiation. As recently reviewed[1], this may be due to Van Allen radiation belt particles or galactic cosmic rays, both of these radiation components being relatively constant with time at a given location of space. Much more variable radiation effects occur due to solar cosmic ray (solar flare ion) events, very energetic electrons, and magnetospheric substorms. These time-variable components introduce a highly fluctuating background into many subsystems onboard a given spacecraft in the earth's outer magnetosphere ($\geq$ 5 R_E). It, therefore, has proven important - indeed, necessary - to monitor such background variations in situ aboard geostationary orbit spacecraft.

A further problem with particle radiations in the outer magnetosphere is the occurrence of spacecraft operational anomalies and upsets due to the presence of energetic particles. This is a problem endemic in the outer magnetosphere, affecting most spacecraft at least to some degree, and requires a continual monitoring of conditions in space. From such monitoring one may rapidly evaluate whether a spacecraft has had a problem related to environmental conditions, or as a result some other sort of cause.

In this paper we will review the present generation of Los Alamos energetic particle sensors being flown at geostationary orbit. We will provide general hardware descriptions as well as demonstrations of some of the data analysis results obtained from the instrumentation. In the latter part of the paper we will describe the next generation of particle instruments presently under development and test. We will show the potential value of these new sensor systems and we will describe the benefits of a proposed real-time data system to analyze and display more promptly the available geostationary orbit particle data.

Present Los Alamos Instruments at 6.6 R_E

The CPA Detector System

The Charged-Particle Analyzer (CPA) is one of a series of instruments develop[illegible] National Laboratory for several [illegible]. The instrument consists of [illegible] detectors; each detector is designed [illegible] specific energy range and particle species and uses one or more semiconductor detectors as its sensor elements. The basic accumulation time for a given energy channel is 8 ms. The data sequence repeats every 256 ms; thus for a nominal 10-s spacecraft rotation period each energy level for each sensor is sampled 40 times.

Electron fluxes are measured by two different detectors: the LoE and HiE units for the low- and high-energy ranges, respectively (see Fig. 1). The LoE detector consists of five separate elements. Each element has a single sensor with a collimating aperture having a half angle of ~2.6° and a geometrical factor of 3.6×10^{-3} cm^2 sr. The view angles of the elements are 0°, ±30°, and ±60° to the spacecraft equatorial plane and thus a large fraction of the 4π unit sphere is sampled by the LoE detector during each spacecraft rotation. The nominal energy levels are 30, 45, 65, 95, 140, and 200 keV with an upper-energy cutoff of 300 keV. The HiE detector scans only in the spacecraft equatorial plane and consists of a collimator-sensor combination having a half angle of 3.7° and a geometric factor of 1.8×10^{-2} cm^2 sr. Nominal HiE threshold levels are 0.2, 0.3, 0.4, 0.6, 0.9, and 1.4 MeV with an upper-energy cutoff at 2.0 MeV (see Table 1).

The LoP and HiP proton detectors (Fig. 2) also scan in the spacecraft equatorial plane; each has an active guard scintillator and a sweeping magnet to eliminate contamination from electrons below ~1 MeV. The HiP uses three sensors in a telescope configuration to cover the energy range 0.4-150 MeV with sixteen differential energy channels. The nominal HiP energy thresholds are 0.4, 0.5, 0.6, 0.8, 1.0, 1.3, 1.7, 2.7, 4.7, 9.0, 13, 25, 38, 50, 78, and 108 MeV. (150 MeV is the upper-energy cutoff.) It should be pointed out that there is variance in the HiP energy threshold for the detectors in orbit. The exact threshold for the LoP instrument also vary for different instruments in the CPA series.

As can be seen in Fig. 2, the low-energy proton sensor consists of a single thin (40 μ) silicon detector (S1) surrounded by magnesium shielding. A plastic scintillator detector (S2) serves as an anticoincidence element to eliminate penetrating particles that enter through the collimator aperture as well as charged particles that enter through the rear of the detector. The sweeping magnet serves to eliminate electrons with

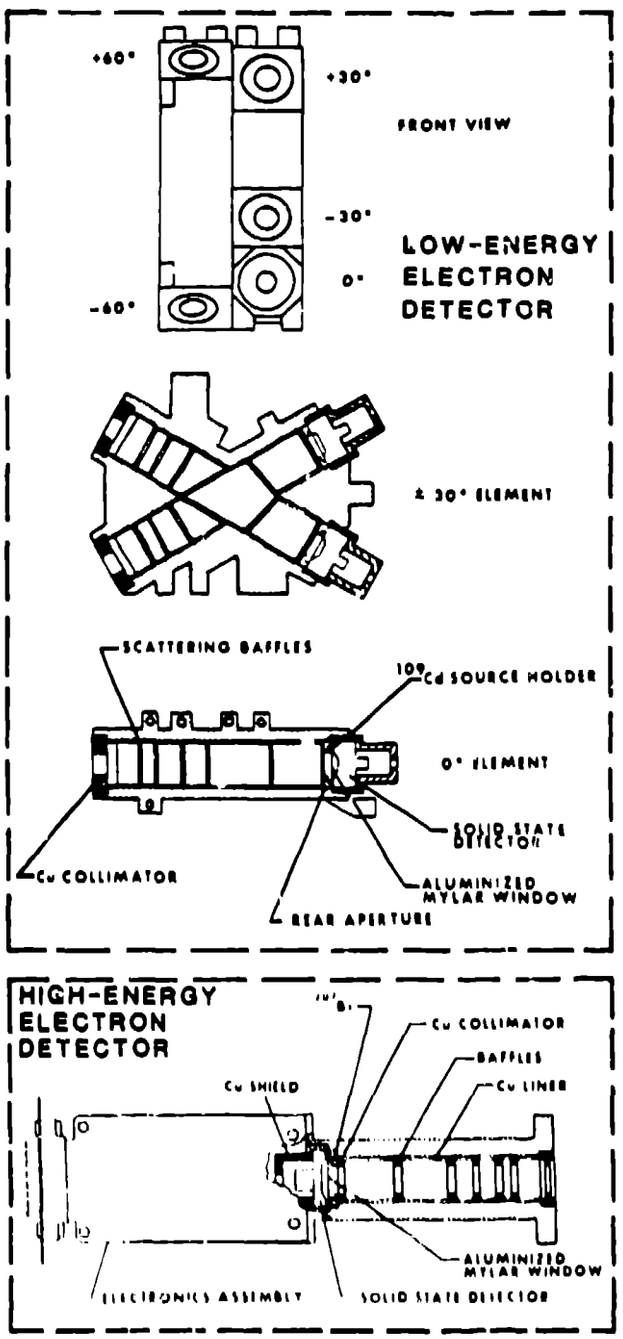

Figure 1. The upper portion of the figure shows the low-energy electron (LoE) detector portion of the CPA including overall arrangement of the five sensors and cross-sectional views of the ±30° and the 0° elements. The lower portion of the figure shows a cross-section of high-energy (HiE) electron detector.

E_e < 500 keV. A light-tight nickel window is interposed between the magnet and S1 in some earlier detectors whereas later models used sensors with additional thickness to the aluminum contact to effect the light-tightness. The effective area of S1 is 0.5 cm^2, and the collimation aperture has an opening half angle of ~2.5°. The resulting geometric factor for the sensor is 3.9×10^{-2} cm^2 sr over the proton detection energy range 100-600 keV.

The high-energy proton telescope shown in Fig. 2 consists of three solid state detectors (D1, D2, and D3) surrounded by a plastic scintillator anticoincidence cup (D4). D1 is a 45-μ surface barrier silicon detector with an effective area of 1.0 cm^2. D2 is a 3-mm-thick lithium drifted detector with an area of 2.3 cm^2. D3 is again a surface barrier detector with a thickness of 500 μ and an effective area of 2.5 cm^2.

The aluminized mylar window (~600 $\mu g/cm^2$ aluminum equivalent thickness) keeps light from striking the detector stack, while the sweeping magnet is designed to prevent electrons with E_e < 1.0 MeV from reaching the telescope sensors. The threshold of D4 is such that all charged particles (not entering through the front aperture) with energy depositions at or above that of a minimum ionizing particle are rejected. The brass collimation defines an entrance aperture for the telescope of ~6.5° half angle.

In the high-energy telescope, proton detection events fulfilling the D1D2D4 logic requirement lie in the energy range $0.4 < E_{p2} < 2.2$ MeV with a geometric factor of 4.4 × 10^{-2} cm^2 sr. Events fulfilling the D1D2D3D4 logic requirement lie in the energy range $2.7 < E_p < 22$ MeV. The geometric factor for D1D2 events is again 4.4×10^{-2} cm^2 sr. Particles which penetrate D2 and are subsequently counted by D3 lie in the energy range $25 < E_p < 150$ MeV. The geometric factor for these protons is ~8×10^{-2} cm^2 sr. Protons with energies greater than 150 MeV penetrate the thick tungsten absorber (see Fig. 2) and hence are rejected by the D4 anticoincidence condition.

The spacecraft rotates with a spin period of ~10 s about an axis which is pointed continuously toward the center of the earth by an active control system. Both the low-energy and the high-energy proton detectors point radially outward in the spacecraft equatorial plane, so that proton measurements are made in a narrow solid angle band in a plane approximately perpendicular to the ecliptic. In the essentially dipolar magnetic field which often exists at 6.6 R_E the CPA proton detectors scan nearly all pitch angles during one rotation. In the highly distorted taillike fields often encountered on the nightside of the magnetosphere, very limited pitch angle scans may result.

The three-dimensional data from the LoE detector are analyzed by making a least squares fit to the observed fluxes using the 200 points obtained from a single energy level during a spacecraft rotation. Spherical harmonic functions are used for this fit and, although they are not eigenfunctions for electron distributions in the magnetosphere, these functions have useful properties which simplify the analysis. The zeroth-, first-, second-, and fourth-order harmonics are computed, but the second-order components are the most commonly used. Since the

Table 1. Charged Particle Analyzer (CPA) Characteristics

Sensor	Particle Species	# Telescopes	Energy Range	# Energy Channels	Geometric Factor
LoE	Electrons	5	30-300 keV	6	3.6×10^{-3} cm^{2}sr
HiE	Electrons	1	0.2-2 MeV	6	1.8×10^{-2}
LoP	Ions	1	100-600 keV	10	3.9×10^{-3}
HiP	Ions	1	0.4-150 MeV	16	4.4×10^{-2}*

*g = 8×10^{-2} cm^2-sr above 22 MeV.

spacecraft does not have an on-board magnetometer, the symmetry axis of the second- or fourth-order fits is used to order the data and is identified with the magnetic field direction. Implicit in this identification are the assumptions that the spacecraft is on a closed field line and that the distribution changes slowly compared with the spacecraft rotation period. Gradient and convection effects would be reflected in the odd order terms. The pair (θ_2, ϕ_2) commonly used[1] corresponds to the direction of the symmetry axis of the second order fit to the distribution in HVD coordinates. In this system H is parallel to the dipole axis, D points eastward, and V is approximately radially outward[2]. This system is also called "dipole meridian." θ_2 is the colatitude with respect to the H axis, and ϕ_2 is the azimuth measured from the negative V axis. C_2 is the amplitude of the symmetrized second harmonic component. $C_2 > 0$ indicates a 'cigar-shaped' distribution (minimum flux at ~90°) and $C_2 < 0$ indicates a 'pancake-shaped' distribution (maximum flux at 90°). Either of these broad categories can also show 'butterfly' characteristics (i.e., two secondary flux maxima). A more detailed exposition of this technique is given in Ref. 3.

The SEE Detector System

Unexplained anomalies occurring in the electronics aboard a number of operational spacecraft at synchronous altitude precipitated a reconsideration of the model representing the trapped radiation environment. In 1977 the Aerospace Corporation proposed a new model, designated AE-7, of the electron environment at synchronous altitude[4]. This model predicts a high-energy contribution much enhanced over the then-current NASA environment model[5]. Although the AE-7 model was based upon data from the ATS and OVI-19 satellites, the population of electrons with energies greater than 1 MeV had not been adequately characterized. These energetic electrons are very penetrating and, thus, very difficult to shield against. In order to better define the populations of electrons at these high energies and their variations over long periods of time, a project was undertaken to provide an electron spectrometer which could be implemented at minimum impact to the existing spacecraft program. This approach provides the advantage of long-duration monitoring with a good duty cycle.

The instrument which was designed to perform this needed measurement is called the Spectrometer for Energetic Electrons (SEE detector). It was designed to be compatible with the mechanical and electrical interfaces provided for another instrument: only ~2 kg of mass was allowed for the experiment, and only five data channels (at a total effective data rate of five bits per second) were available. Sufficient electrical power (0.5 watt) was provided to accommodate the measurements possible within the constraints of the data handling system.

In order to accommodate the desired measurement within these constraints, the instrument was based upon a scintillation spectrometer in which essentially all of the energy of the incident electrons is deposited and measured. Silicon solid-state detectors are used to determine that a response in the scintillator is caused by an electron entering the detector though a collimating aperture (Fig. 3). Except for the aperture, the detector is shielded by a thick (5 gm cm^{-2}) aluminum shell, which prevents the direct penetration of electrons with energies less than ~15 MeV. The detector is powered through a self-contained power converter the housing of which also serves as the mounting base for the instrument. The electronics which process the response of the detector and present the results to the data handling system are housed in an enclosure which is mounted to the sensor shell.

The silicon solid-state detectors which provide the gating signal enabling the measurement of the total energy of the electron being analyzed consists of a stacked pair of elements, electrically connected in parallel. Early flight detectors employed 1500 μ ion-implanted sensors in order to allow a gating threshold sufficiently high (0.9-1.3 MeV window) so that the random counting rate and the probability of random coincidences between lower-energy particles would not produce an unacceptably high random background in the gating channel. Later detectors were equipped with 1000 μ ruggedized surface-barrier sensors with the addition of a passive aluminum absorber immediately covering the front element in order to maintain the singles rate within acceptable limits. Additionally, electrons are required to penetrate an aluminum honeycomb panel, losing ~0.3 MeV

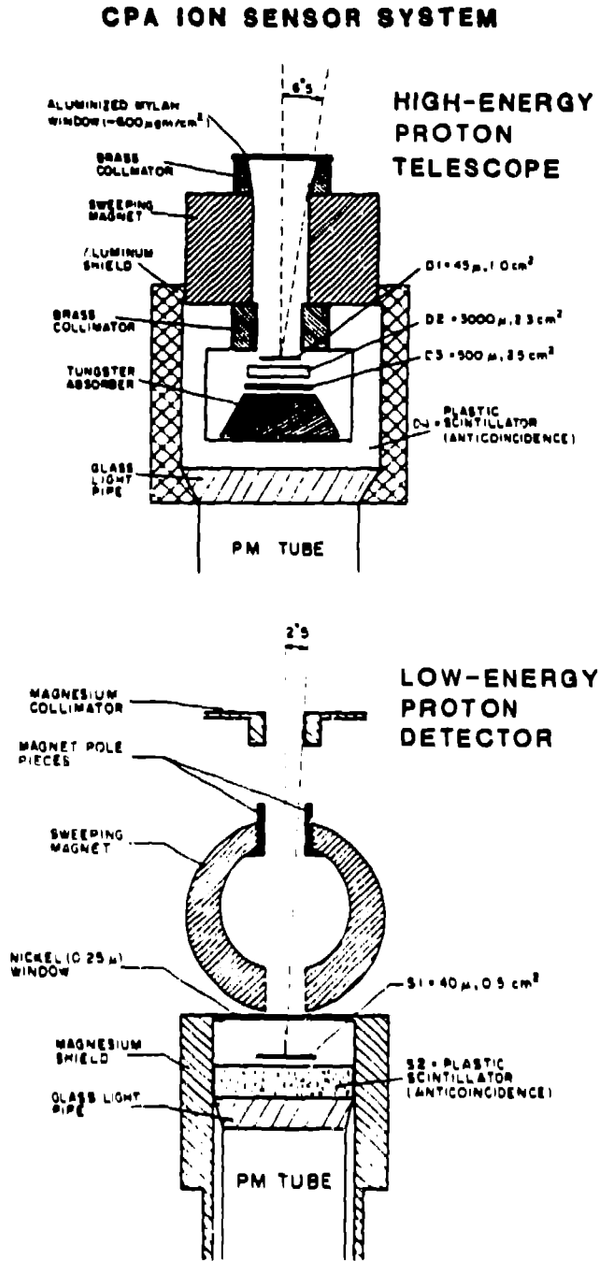

Figure 2. Cross-sectional schematic illustrations of the low-energy proton (LoP) and high-energy proton (HiP) portions of the CPA sensor system.

energy, before entering the collimating aperture of the detector.

The scintillation spectrometer, where the energy remaining to the electron (after penetration through the gating sensor) is deposited, is based upon a 1.25" x 1.25" bismuth germinate (BGO) scintillator. BGO was chosen in order to maximize stopping efficiency and re-collection of bremsstrahlung generated in absorbing the kinetic energy of the electron (within the limited volume and mass available), at the cost of some increase

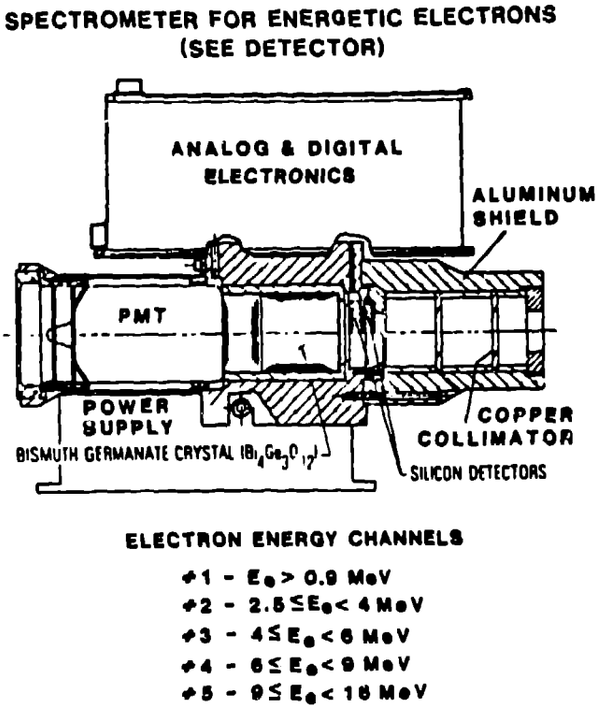

Figure 3. A diagram of the SEE detector system illustrating the collimator, the silicon detector arrangement, and the BGO (bismuth germanate) crystal. Particle detection characteristics are also shown.

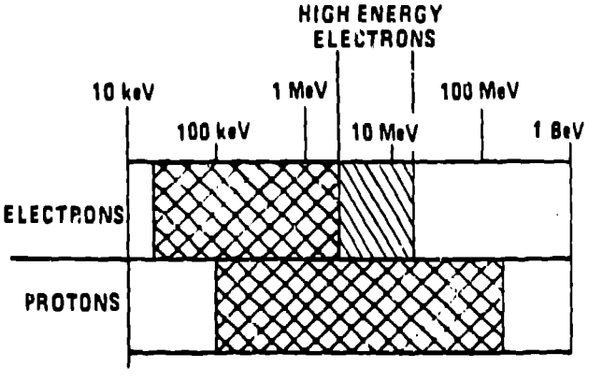

Figure 4. An illustration of the overall electron and proton energy ranges measured by present-generation Los Alamos sensors at geostationary orbit.

in backscattering from the detector. A 0.050" lead shell surrounds the scintillator, shielding it from much of the bremsstrahlung generated in the spacecraft and at the surface of the instrument itself by the trapped-radiation environment. A leaded-glass lightpipe completes the shielding surrounding the scintillator and couples the scintillator to an RCA type 7151Q photomultiplier (PM) tube. High voltage required to operate the PM tube is generated in the power converter and is controllable, by command, to vary the gain of the PM tube over eight discrete levels.

Electrical signals developed in the PM tube are amplified and analyzed at five levels, determined by discrete level discriminators. The total scintillation detector counting rate may be monitored from the output of the lowest-level discriminator. Counting rates occurring within the differential interval defined between adjacent level discriminators require logical coincidence (or lack of coincidence) with response from the silicon gating detectors, thus providing a measurement of electrons with energies in four differential intervals as shown in Fig. 3. A commandable function selection permits reduction of this primary measurement to only three channels, utilizing the fourth channel to monitor the total counting rate from the scintillation detector.

The silicon gating sensors are electrically connected in parallel. Signals from the sensors are amplified by a charge-sensitive preamp followed by a voltage amplifier. Two level discriminators define energies of ~90% and ~150% of the most probable energy deposited by electrons within the measurement range. This provides >90% efficiency in identifying the entrance of these electrons through the collimator aperture.

It has been difficult to provide satisfactory calibrations of the instrument, because of the energy range in which it is designed to perform its monitoring functions. Monte-Carlo design studies have been done to simulate actual detector response. At energies greater than 2 MeV, the electrons are not stopped cleanly, but produce many secondary interactions as their energy is dissipated. An appreciable number of electrons are scattered backward, escaping the scintillator. Others lose energy primarily by generating bremsstrahlung, some of which escapes the scintillator. Additionally, the resolution of the scintillation detector smears the response, however, this was not accounted for in the current analysis. Actual calibrations of the detector have been performed utilizing electron beams provided by a linear accelerator. Results of the calibrations are in reasonable agreement with the Monte-Carlo simulations.

Figure 4 summarizes the present overall electron and proton energy coverage of the CPA and SEE detector systems.

CPA and SEE Science and Engineering Results

CPA data acquired from 1976 through 1978 were processed by a set of "Phase I" analysis codes. The basic directional count rate arrays were analyzed on a spacecraft rotation basis, particle anisotropies were computed, and spin-averaged fluxes were displayed on 2-hr per frame microfiche plots. Thus, a high time resolution (10-s) archival data set was formed. In addition, as part of the processing, CPA data were stored and averaged to form one-hour and daily flux averages. These latter, courser average data have been used in a variety of statistical studies.[6,7]

From 1979 to the present the CPA data have been processed under a set of "Phase II" computer codes. In addition to the 10-s fiche plots which are nearly identical to the Phase I output, Phase II programs have also produced a one-minute average digital archive of all data products, plus summary 12-hr color spectrogram survey plots. A recent paper illustrates most of the available CPA data products and formats.[8]

The SEE data are available in highest time resolution as 16-s average count rates. These have been averaged to form a 12-min average data set and daily averages have also been formed. Microfiche plots of all average daily energy spectra are available from 1979 to present.[7]

Hot plasma and energetic particle populations are known to produce spacecraft operational anomalies.[1] In the inner part of the earth's magnetosphere, these effects are primarily due to durably trapped radiation belt particles, the integrated doses from which can be calculated accurately for a given orbit. In the outer magnetosphere many spacecraft operational difficulties appear to be due to intense, transient phenomena. The CPA and SEE sensor systems provide energetic particle detection and assessment capabilities during these kinds of high-energy radiation events. As has become increasingly clear, modern satellite systems, weather and global communication installations, and many defense programs have become dependent on knowledge of the condition of the near-earth space environment. Military spacecraft, commercial communication satellites, and a wide variety of other scientific and operational space systems require information about solar and ionospheric conditions, magnetospheric disturbance levels, and solar and galactic cosmic ray fluxes. Without such knowledge, these systems often cannot be operated properly. Three primary forms of radiation affect spacecraft systems in the outer magnetosphere. These are:

(1) Solar flare particles;
(2) Very high energy electrons; and
(3) Magnetospheric substorm particles.

The damaging component of solar flare particles is primarily ions (mostly protons) of 10 to ~200 MeV kinetic energy. The very high energy electrons are 2-20 MeV in kinetic energy and their origin is at present unknown. The third source, the magnetospheric substorm, produces large fluxes of low-to-moderate energy ions and electrons; the mechanisms of damage is primarily one of surface and near-surface spacecraft charging effects.[9]

High Time Resolution CPA Results

The occurrence of large flares on the sun's surface have long been known to be followed after a few hours to a few days by significant geomagnetic disturbances. The nature of the terrestrial effects can include large magnetic storms,

ionospheric disruptions, and intense surface effects.[10] It is now known that flares typically produce very energetic particles and also often give rise to strong travelling shock waves in the interplanetary medium. Given a proper interplanetary magnetic field (IMF) connection between the flare site on the sun and the earth, 10s of MeV solar protons can reach the terrestrial environs in a matter of hours. At earth, these very energetic protons appear to have ready access to the polar cap regions and the outer magnetosphere and, thus, there can be very prompt effects from solar flares.

The damaging aspects of solar flare particles on spacecraft comes in significant measure from fluence effects. Protons in the ten to several hundred MeV range are very penetrating, and one large flare can be as damaging as years of on-orbit operation in the normal, ambient magnetospheric environment. Intense long-term exposure to high-energy proton fluxes produces crystal-lattice structure damage in solid state devices, and beyond a certain point such devices become completely dysfunctional.[11] The effects of large dosages of heavily ionizing radiation on electronics has been well-investigated and damage-fluence curves are available in many cases. The number of rads at which individual components fail varies substantially (depending on device construction), but with sufficient exposure most modern space electronic systems suffer at least some degradation.

Solar flare protons can also produce other types of disturbances in spacecraft systems. For example, data from a geostationary orbit satellite during the early part of August 1972 (J. B. Blake, private communication, 1983) established that when the <50 MeV flux was above ~200 protons $(cm^2\text{-}s)^{-1}$ there was continuous disruption of the onboard star sensor photomultiplier.

The mechanism of disruption in this case was the penetration of the energetic protons into the star sensor system itself. The energy deposition by the protons produced continuous "scintillations" in the photomultiplier system which completely incapacitated the star reference function. Without accurate rotational reference, many operational spacecraft are quite restricted in their performance. This, and a variety of other proton-induced disruptions, have been traced directly to flare-generated particles. Such flare induced backgrounds are continuously monitored by the CPA.

Solar flares occur rather commonly (perhaps once a month) near solar sunspot maximum, but they occur very infrequently near solar minimum. In contrast to the relatively infrequent, but quite energetic, phenomena associated with solar flares, magnetospheric substorms occur much more frequently. During average conditions, there may be one to several isolated substorms (of about 1 hour duration) during a day. During very disturbed, stormlike conditions, substorm activity may be nearly continuous.

One of the most significant effects of substorm from the standpoint of spacecraft operations is the occurrence of spacecraft charging.[9] During a charging event, insulated surfaces may charge to several kilovolts (normally negative relative to the ambient). This charging effect occurs because of a lack of current balance between the ambient plasma medium and the spacecraft surface.[12] Typically when a spacecraft is immersed in a cool, dense plasma then incident electron and ion currents, secondary emitted currents, photoelectrons, and backscattered electrons all balance giving a low potential. However, in a very hot, tenuous plasma, current balance can be hard to achieve and large potentials can build up.

There have been many upsets, anomalies, and disruptions of spacecraft at (or near) synchronous orbit.[13] Hundreds of examples have been observed that show that episodes of large spacecraft charging occur during substorms. Many of these charging events end with abrupt, intense discharges and arcing between spacecraft components. When this occurs, significant damage can occur.[1,9] The vast majority of anomalies and upsets occur in the local time sector from midnight to local dawn. This is the region of substorm energetic electron injection and subsequent drift.[14] The association of many spacecraft operational problems near synchronous orbit with substorm electron flux increases, therefore, is irrefutable.

Particle fluxes at 6.6 R_E regularly decrease about 1 hour before substorm onset and this has been termed the "storage" phase or "growth" phase of the substorm since energy is being added to the magnetotail at these times. Particle drift-shell splitting effects at 6.6 R_E produce a depletion of 90° pitch angle particle and hence a magnetic field-aligned, or "cigar," electron pitch angle distribution is seen before most substorm onsets. Thus, this presubstorm period also has been termed the cigar phase.[15] In studying hundreds of substorm events near local midnight with geostationary spacecraft instruments, we have found that most substorm injection events are preceded by cigar (growth) phase features. Of more than 100 cases of detected cigar phases of ~0.5-3 hour duration, in 97 cases the cigar phase was immediately followed by a substorm injection.[14] On the other hand, when there was no cigar phase throughout the passage of the spacecraft through the local midnight sector, we saw no substorm (as manifested in the energetic particle data) on 15 of those occasions, and we saw weak substorm activity on 2 occasions. Such results from the CPA suggests that substorms tend to occur if, and only if, the cigar phase signatures and magnetotail energy storage occur. This can be the basis of a valuable substorm prediction method (or component thereof) as has been previously suggested.[16]

Long-Term CPA and SEE Results

The existence of populations of very high energy ($\geq$ 2 MeV) electrons deep in the earth's radiation belts have long been known.[5] These electrons constitute a primary integrated dose (fluence) problem for operation of spacecraft below ~4 R_E altitude as was mentioned previously. It has been widely believed, however, that the intensity of such particles dropped off very rapidly with geocentric distance[5] such that little flux remained beyond L ~ 5.

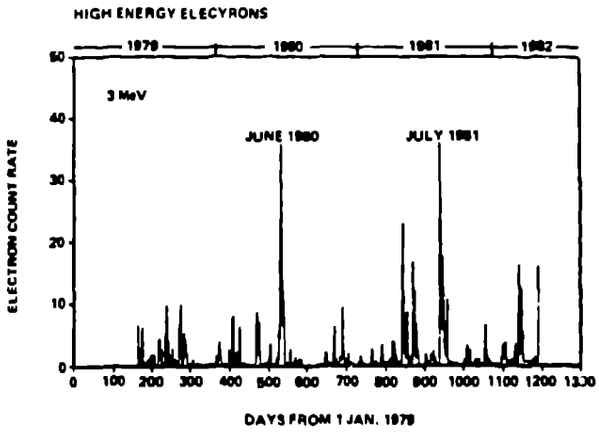

Figure 5. Daily-average, 3-5 MeV electron count rates from June 1979 to April 1982 measured by the SEE detector at 6.6 R_E. Numerous intense spikes, well above normal background levels are seen in the data.

New measurements since 1979 using the SEE detector have shown the sporadic appearance of large fluxes of 2 ~ 10 MeV electrons near synchronous orbit. Figure 5 shows a plot of the daily-average intensity of 3-5 MeV electrons from June 1979 to April 1982. (We refer generally to this population as the ~3 MeV flux.) The data are presented as differential count rate versus day of year from the beginning of 1979.

The data show that much of the time, fluxes of 3 MeV electrons are rather low ($\lesssim$0.1 c/s ~ 1 e^-/cm^2-s-sr-MeV). However, on many occasions the fluxes reach significant levels (~10 c/s); on relatively rare occasions, such as June of 1980 or July 1981, we see extraordinarily high fluxes.

Figure 6 shows a plot of the electron energy spectra for selected days during the June 1980 event. The spectra combine data from the CPA low-energy electron sensor system (30-300 keV) with the high (0.2-2.0 MeV) and very high (2-10 MeV) energy sensor systems on the same geostationary spacecraft. For reference, the short-dash long-dash curve in Fig. 4 shows the NASA AE-4 model environment at 6.6 R_E.[5]

The figure shows that the model environment exhibits a rapid drop-off of flux above ~2 MeV. By contrast, the observed daily average fluxes in the large June 1980 event follow a hard exponential spectrum up to 10 MeV. Thus, while the integral flux above 2 MeV for the AE-4 model would be a few hundred electrons $(cm^2\text{-s-sr})^{-1}$, during the June event we observed $\gtrsim 10^4$ electrons $(cm^2\text{-s-sr})^{-1}$ above 2 MeV. The model predicts essentially no measurable fluxes above ~5 MeV whereas we observe differential fluxes roughly five orders of magnitude higher than the model at these energies.

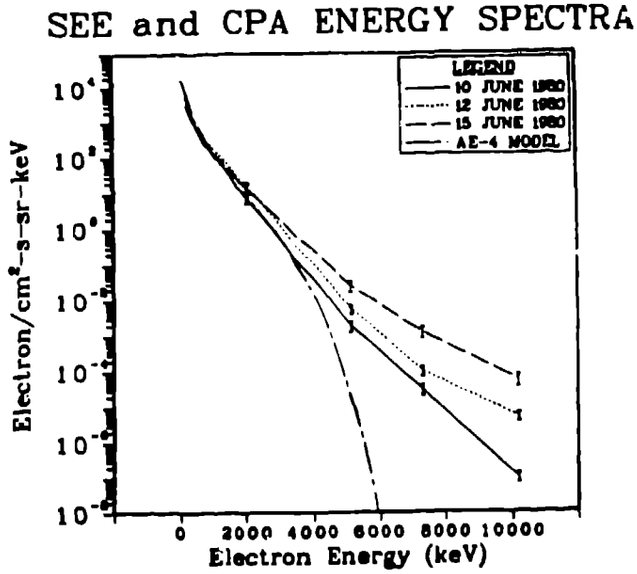

Figure 6. Composite CPA and SEE spectra from 30 keV to ~10 MeV for three selected days during an intense electron event in June 1980. For comparison, the NASA AE-4 environmental model is shown. These results illustrate that the high energy electron fluxes at 6.6 R_E often greatly exceed the nominal model predictions.

The occurrence of very high energy electrons at 6.6 R_E is of significant engineering interest. We have found numerous examples of spacecraft operational problems occurring during such flux enhancements.[1] One class of anomalies for which the high energy electron component is clearly implicated has been well-studies. During a broad interval of time (October 1980 - April 1982) the star tracker system onboard a geosynchronous satellite experienced repeated outages and malfunctions. Typically, there were several days of erratic behavior after which the problems would disappear. The star tracker upsets occurred essentially whenever fluxes of electrons exceeded an approximately empirical level of 6 count rate units. Further, star tracker disruptions never were seen when fluxes remained below this empirical level. The high degree of correlation between star tracker upsets and very energetic electron fluxes is strong evidence for a causal relationship between the environment and the anomalies.[1]

It has been shown[1,7] that irradiation of space systems by very energetic electrons can cause a deep dielectric charging phenomenon. Essentially, very high energy (i.e., very penetrating) electrons can bury themselves in dielectric materials (e.g., coaxial cables, etc.) and stop. They then give rise to very high electric fields (potential differences of several kilovolts) in these regions until eventually an intense breakdown occurs. Hence, a nearly irrefutable correlation of spacecraft anomalies with the environment exists and, further, a plausible physical connection can be established.

Unfortunately, it is very hard to shield against multi-MeV electrons. The greatest hope is to be aware that such particles occur rather regularly at 6.6 R_E and to design systems and subsystems which are immune to their effects. From the standpoint of predictions, we are finding considerable evidence that this very energetic component recurs with a regular 27-day (solar rotation) periodicity[6], and thus we should eventually be able to predict the times of their occurrence reasonably well.

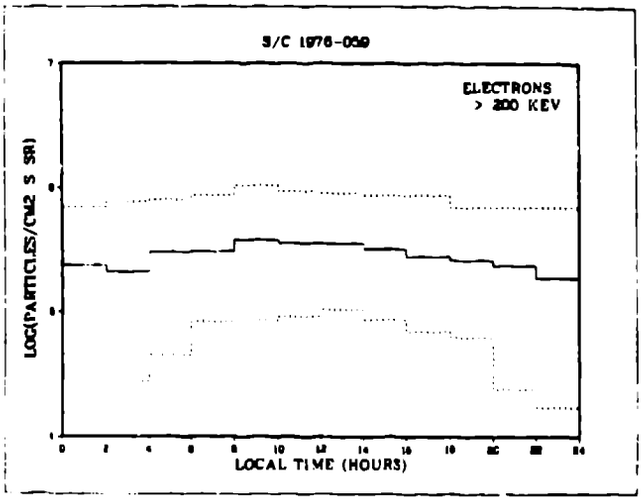

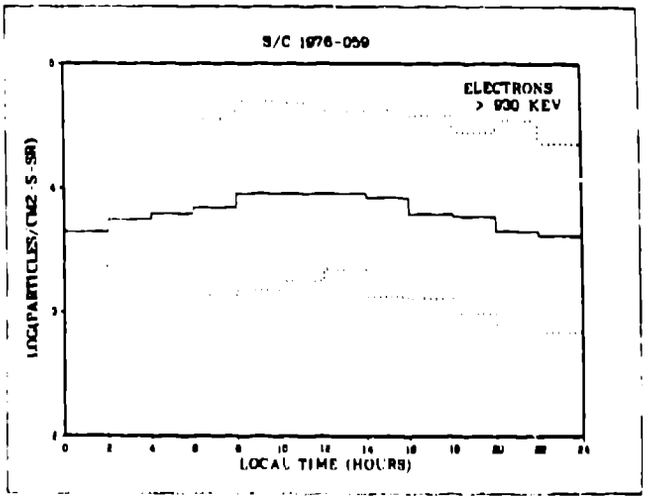

Figure 7. Plots of the average diurnal variations of fluxes of electrons (>200 keV and >930 keV) measured by S/C 1976-059 during the years 1976 through 1978. The solid line in each plot illustrates the mean flux (50% probability) value. The upper dashed curve in each case shows the flux level that is exceeded only 10% of the time; the lower dashed curve shows the flux level that is exceeded 90% of the time. These sorts of results allow one to judge what the likely average as well as extreme conditions of low flux or high flux might be.

A final illustration of the scientific and engineering results from the Los Alamos geostationary orbit data set is shown in Figure 7. This is based on the kinds of broad statistical analyses which have been performed on the CPA and SEE data sets.[7,8] In the figure we illustrate the average diurnal variations of energetic electrons observed in two energy ranges (>200 keV and >930 keV) during 1976-1978. The plots utilize all data available from S/C 1976-059 and the statistical evaluation used the 1-hr data tapes as input. In Fig. 7 we have plotted the mean flux (50% probability) value as well as the 10% and 90% flux probability values for each channel. From such curves, it is possible to judge what the average energetic particle environment at 6.6 R_E would be (for any given local time). It is also possible to judge what the likely extreme conditions of either low flux (90% probability) or high flux (10% probability) might be. Results of these kinds should be useful in an engineering sense and should allow assessment of flux levels important for spacecraft design criteria.

New Generation Los Alamos Particle Instruments

The APO System

The Advanced Particle Analyzer (APO) instrument will analyze electron fluxes with essentially the same energy range and resolution as the present CPA instrument, and cover the protons with about one-half the energy resolution. The ion energy range will be shifted considerably to the lower energy side. In addition, the APO will have the capability of monitoring the fluxes of helium, carbon, nitrogen, oxygen and other heavy ions whose existence and function in magnetospheric processes are only now beginning to be determined. The APO will also have three-dimensional pitch angle capability for electrons, protons and alphas whereas the current CPA is limited to electrons in this respect (see above).

The APO instrument consists of a set of three collimated semiconductor sensor telescopes (see Fig. 8). The axes of the collimators are located an angles of 0 degrees, +60 degrees, and -30 degrees with respect to the spacecraft equatorial plane. The electron pitch angle distributions are symmetric for the trapped electron population at geostationary altitudes, so this arrangement gives high pitch angle coverage and maximizes the heavy ion coverage which peaks strongly near 90 degrees. Each telescope consists of a pair of solid state sensors in an E - dE/dX arrangement. The front element of the telescope is a surface barrier sensor 4 microns thick and 10 mm^2 in surface area. It has a capacitance of > 250 pF and operates with 1.5 volts of bias. The back element of the telescope is a surface barrier sensor 3000 microns thick and 25 mm^2 in surface area with a capacitance of a few picofarads and operating bias voltage of approximately 900 volts.

The APO detector is designed to measure ions in the 50 keV to 50 MeV energy range and electrons in the range from 50 keV to 1.6 MeV with an integral channel >1.6 MeV. Specifically, the ion measurements include protons (50 keV - 50 MeV), alpha particles (500 keV - 1.5 MeV), carbon, nitrogen and oxygen ions (1.5 MeV - ~25 MeV) and heavier ions (>7 MeV). The protons will be counted

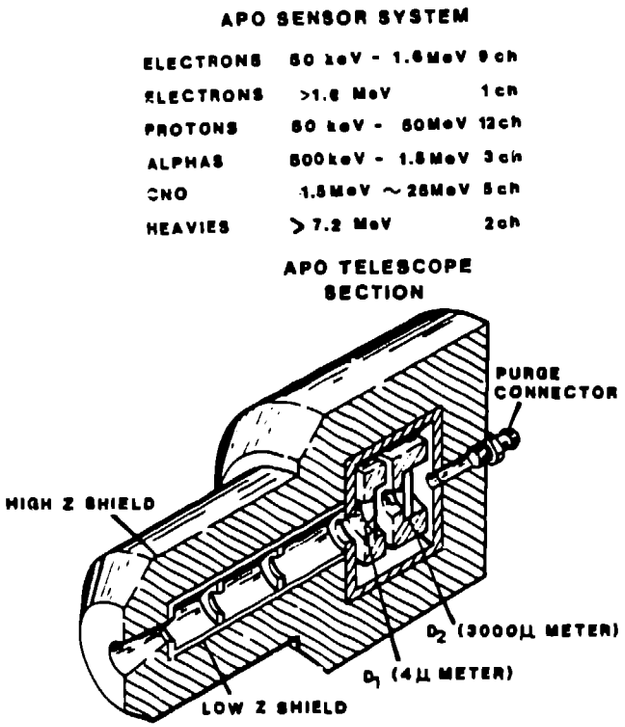

Figure 8. A diagram of one of the individual APO sensor telescopes and the measurement energy ranges for electrons, protons, and heavier ions.

in 12 differential energy channels, the alpha particles in 3 channels, the CNO ions in 5 channels and the heavy ions in 2 channels. The 5 CNO channels include 2 channels in which carbon, nitrogen, and oxygen are counted together and one channel each in which they are counted uniquely. Electrons are counted in 9 differential energy channels and 1 integral channel.

Sixty-four (64) angular samples will be acquired over the unit sphere for electron, proton, and alpha channels during a 10.24 second period (essentially one spacecraft rotation). Thus data will be accumulated in all of these channels for 160 milliseconds. Since the counting rates for the heavier ions (CNO and heavier ions) are very low, the accumulation time for these channels will be 10.24 seconds (approximately one spacecraft rotation).

In order to make a more accurate heavy ion composition measurement over longer time scales, a dual parameter analysis will be performed on the dE/dX pulse heights due to heavy ions passing through a particular telescope. The valid pulse pairs will be digitized and the data transmitted to and accumulated on the ground. Pulse pairs generated during the time a telescope sweeps across the sun (sun sensor monitor is set = 1) will be invalidated by the ground processor.

Each pair of solid-state sensors in the set of three telescopes have an associated charge sensitive preamplifier; however, to conserve both weight and power, the three telescopes share the same post electronics and logic. Thus, there are two postamplifier chains, one for each of the two elements in a telescope. The amplifiers are followed by energy level discriminators, differential scaling logic, particle identification logic, and accumulators for each of the ion and electron channels. There are a total of 22 ion channels and 10 electron channels.

Since the telescopes must share the post electronics, each telescope will be selected in a fixed pattern every 160 milliseconds with the 0 degree telescope selected twice as often as the other two. Thus, the 0 degree telescope will have a 50% duty cycle while the +60 degree and -30 degree telescope will each have a 25% duty cycle. Accumulations are made for 160 mseconds as mentioned above and the +60 degree and -30 degree telescope will have a resolution of 640 mseconds and the 0 degree will have a resolution of 320 mseconds. The dual parameter composition measurement will be made on a continuous basis with the data tagged to the T1, T2 and T3 telescopes. Up to 50 pulse pairs can be accumulated each second.

The ASEP Detector System

The Advanced Spectrometer for Energetic Particles (ASEP) detector assemblies each contain a

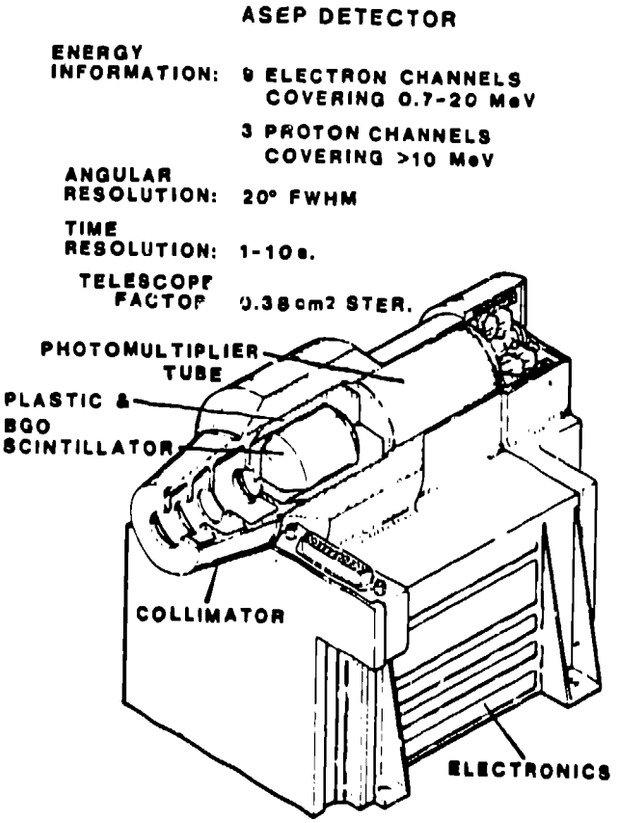

Figure 9. A cutaway diagram of the ASEP sensor system and a tabulation of its physical characteristics and the response to electrons and protons.

scintillator, PM tube, power supply, and electronics (see Fig. 9). The detectors are based on Bismuth Germanate (BGO) and plastic (NE102) scintillation spectrometers. The plastic scintillator surrounds the BGO to provide active charged particle shielding which is supplemented by passive shielding (1/2 inch AL) effective to 6 MeV for electrons and 50 MeV for protons. The active charged particle discrimination is achieved by phoswiching, i.e., optically bonding both scintillators to the same photomultiplier and separating their responses via rise time analysis. An aperture in the passive shield allows a 1.8 cm^2 area of the NE102 to act as a charged particle window, thus performing the same function as the solid state sensor in the present SEE detector, but with less complexity and higher reliability.

The ASEP instruments operate as follows: Pulses from the BGO/NE102 scintillator are categorized according to pulse rise time as either "fast" (NE102) or "slow" (BGO) or as a fast/slow combination. All pulses are further subdivided into classes according to pulse amplitude. All this is done with four level discriminators. The type of radiation that caused the pulse is determined by the level discriminators that trigger. The analog-to-digital converter (ADC) measures the energy deposited per pulse. Electrons from ~1 MeV to ~15 MeV can be measured, while protons from ~10 to ~200 MeV are also counted separately.

In-flight calibration is partially accomplished by continuously monitoring the pulse amplitude distribution due to primary cosmic rays. A series of pulses are injected into the detector analog circuitry for the purpose of more precisely verifying the ADC converter calibration and logic operation.

The heart of the detector electronics is the rise-time discrimination circuit. This circuit separates the mix of fast (10 nsec) and slow (500 nsec) pulse components appearing at the output of the PM tube. The fast component is isolated by a fast preamplifier which has an integration constant much shorter than the 500 nsec rise time of the slow component. The slow component is then isolated by subtracting the fast component from the composite pulse.

The fast signal is amplified and applied to two level discriminators. The slow signal is amplified and digitized by a 15-level ADC converter. Either level 1 or level 3 of the ADC converter is remotely selected to serve as the slow lower level discriminator and level 8 is the slow upper level detector. The combination of the four level discriminators which are triggered by an event and the energy deposition measured by the ADC converter identify the radiation type (see Fig. 9). This determination is made in the ASEP logic located in a separate assembly.

Overall Advanced Sensor Systems Capabilities

In addition to the APO and ASEP systems described above, the next generation of Los Alamos instruments will also include an Advanced Plasma Spectrometer (APS) instrument. This detector system consists of a hemispherical electrostatic analyzer based extensively on prior Los Alamos plasma detection techniques. The APS will measure separately the fluxes and spectra of electrons and ions from ~1 eV to 40 keV. These measurements will obviously complement the APO measurements very well at the lower energy part of the total environment spectral range.

Figure 10 shows the combined Los Alamos advanced sensor system capability at 6.6 R_E. This is to be compared with present capabilities as shown in Fig. 4. From this figure it is seen that virtually the entire electron spectrum from 1 eV to ~15 MeV is covered (with a small gap between 40 keV and ~50 keV). Similarly, the ion spectrum is covered from ~1 eV to ~200 MeV except for a small gap between the APS and APO ranges. Note in particular that the APS/APO coverage should provide excellent data concerning spacecraft charging problems. Similarly, the APO and ASEP combination should provide excellent data concerning solar flare protons and very high energy electrons.

Summary and Future Directions

The geostationary orbit is a region of considerable human interest in space. At this location, a spacecraft appears to remain fixed above a given point on the earth's geographic equator as the orbiting satellite completes one revolution while the earth completes one daily rotation. This orbit is therefore very useful for many satellite applications to weather, communication, and military needs when it is desirable for a spacecraft to maintain a constant position relative to particular geographic locations or land masses.

Scientifically, 6.6 R_E is also a very interesting position within the terrestrial magnetosphere. The geostationary orbit is at the

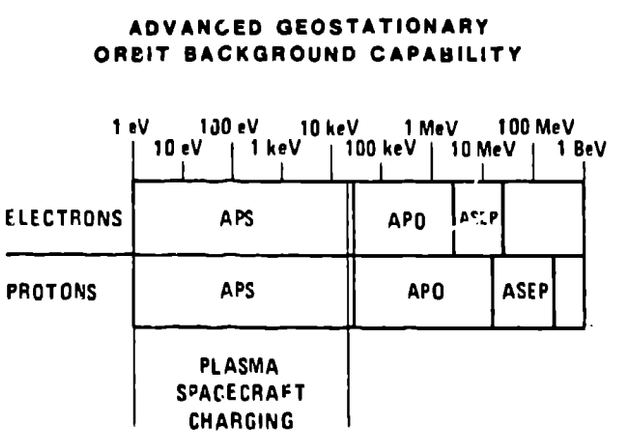

Figure 10. An overall summary of the Los Alamos advanced geostationary orbit particle detection capabilities. In combination, the APS, APO, and ASEP sensors cover virtually all of the electron spectrum up to ~20 MeV and nearly all of the proton spectrum up to ~200 MeV. In particular the APS system measures in a range not covered by present systems (See Fig. 4) that is important for spacecraft surface charging problems.

outer terminus of the terrestrial trapped radiation region (outer radiation zone) and is also at the inner edge of the magnetotail plasma sheet. From a geostationary spacecraft platform, therefore, scientific instrumentation can probe the highly dynamic outer magnetosphere and can assess both the trapped (Van Allen) radiation environment and plasma sheet conditions, the latter being strongly modulated by geomagnetic activity.

From 1976 for the CPA (and from 1979 for the SEE) up to the present time, Los Alamos instruments have provided a nearly continuous record of the energetic particle environment at 6.6 R_E. We expect this record to continue into the future with an even more comprehensive data set. As shown in this paper, the instrumentation is well-suited for overall environmental monitoring, and the results have been of significant scientific and engineering value.

There exists a large and diverse "applications community" by which we mean those persons and organizations who are using the atmosphere and/or outer space for commercial, engineering, or military purposes. This community often needs to know the geomagnetic and magnetospheric environmental conditions to better carry out its tasks (that is, spacecraft design, communication, or satellite operations).

We believe that the statistical studies of the type discussed in this paper are particularly useful for this community. Our statistical results clearly indicate the sorts of flux levels of energetic particles that may be expected to be encountered at geostationary orbit. The probability levels assigned to various flux levels of the different particle components should allow better assessment of design criteria for future geostationary satellite missions, as an example.

We expect that the overall particle data set can also be useful in evaluating events of interest to the applications community long after these events have occurred. For example, spacecraft operational anomalies or atmospheric disturbances (affecting radio propagation) can at times be interpreted in terms of energetic particle enhancements in the outer magnetosphere. The data presented here (and data that continue to be collected by CPAs and SEEs on orbit) are readily available for use by the applications community. Data are also available from these satellites in real time for qualified users in the applications community for environmental monitoring purposes.

Within the scientific community, a major goal is to better understand magnetospheric structure and dynamics. Relevant questions include where energetic plasma particles originate, how the particles are subsequently transported, and how they are eventually lost (precipitated into the terrestrial atmosphere). Long-term fluxes such as given by the present data can lead to a better predictive capability in the future.

We envision that an expanded real-time data system involving all of the Los Alamos geostationary orbit data could be of considerable value. We are, therefore, actively pursuing such an objective. Our basic approach is to streamline and unify data acquisition from each of the particle sensor subsystems. Through this means we foresee the enhancement of the handling of these data as an overall spacecraft operation tool.

Our objectives in developing a real-time data system are to provide resident Los Alamos expertise for space environmental evaluation and to develop a prediction and environmental assessment capability for improved spacecraft operation throughout the terrestrial magnetosphere.

Among the tangible benefits that will accrue for these efforts are:

(1) A magnetospheric substorm prediction algorithm;
(2) Implementation of a workable spacecraft charging algorithm;
(3) Analysis of spacecraft operational anomalies on short (< 1 day) time scales;
(4) Elimination of obsolescent data acquisition systems; and
(5) A reduction of data handling manpower and tape handling.

We conclude that background environmental sensor systems at geostationary orbit have broad and valuable scientific and engineering applications. The use of data from such systems can be of considerable benefit over a wide spectrum of operational conditions. Thus, such data are, and will continue to be, a powerful resource in the continuing use of near-earth space.

Acknowledgments

We thank the many individuals at Los Alamos and Sandia National Laboratories who have made the CPA, SEE, and related programs a success. This work was supported by the U.S. Department of Energy.

References

1. Baker, D. N., in press in Proceedings of the Solar-Terrestrial Predictions Workshop, Meudon, France, 18-22 June 1984.

2. McPherron, R. L., EOS Trans. AGU, 56, 614, 1975.

3. Higbie, P. R., and W. R. Moomey, Nucl. Inst. Methods, 146, 439, 1977.

4. Vampola, A. L., et al., J. Spacecraft and Rockets, 14, 690, 1977.

5. Fette, J. I., et al., Solar-Terrestrial Predictions Proceedings, Vol. 2 (ed., R. F. Donnelly), p. 21, NOAA, Boulder, CO, 1979.

6. Baker, D. N., et al., Geophys. Res. Lett, 6, 531, 1979.

7. Baker, D. N., et al., Los Alamos National Laboratory report LA-8843, August 1981.

8. Baker, D. N., et al., in The IMS Source Book (C. T. Russell and D. J. Southwood, Eds.), p. 82, Am. Geophys. Union, Washington, D.C., 1982.

9. Rosen, A. (Ed.) Spacecraft Charging by Magnetospheric Plasmas, AIAA, Vol. 47, New York, 1976.

10. Paulikas, G. A., and L. J. Lanzerotti, Rev. Sp. Sci., p. 42, July/August 1982.

11. Bouquet, F. L., et al., IEEE Trans. Nuc. Sci., NS-30, p. 4090, 1983.

12. DeForest, S. W., J. Geophys. Res., 77, 651, 1972.

13. McPherson, D. A., et al., Spacecraft Charging at High Altitudes - The SCATHA Program, AIAA, p. 75, 1975.

14. Baker, D. N., in Magnetic Reconnection in Space and Laboratory Plasmas (E. W. Hones, Ed.), p. 193, Am. Geophys. Union, Washington, D.C., 1984.

15. Baker, D. N., et al., J. Geophys. Res., 83, 4863, 1978.

16. Baker, D. N., et al., J. Geophys. Res., 84, 7138, 1979.

17. Reagan, J. B., et al., IEEE Trans. Elec. Insul., EI-18, p. 354, 1983.